Effects of BaRuO3 addition on hydrogen desorption in MgH2

Effects of $BaRuO_3$ addition on hydrogen desorption in MgH_2

M. Baricco[1,*], M. W. Rahman[1], S. Livraghi[1], A. Castellero[1], S. Enzo[2], E. Giamello[1]

[1]Dipartimento di Chimica IFM and NIS, Università di Torino, Via P. Giuria 9, 10125, Torino, Italy

[2]Dipartimento di Chimica, Università di Sassari, Via Vienna, 2, 07100, Sassari, Italy

[#]Corresponding author: marcello.baricco@unito.it

Keywords

Hydrogen storage; oxide bronze; MgH2; BaRuO3; kinetic analyis.

Abstract

Hydrogen storage in MgH_2 is strongly limited by kinetic constraints, so that several additives have been considered in order to improve the rate of hydrogen desorption. The present work is devoted to investigate the effect of $BaRuO_3$ addition on hydrogen absorption and desorption properties of MgH_2. $BaRuO_3$ was prepared by solid-state synthesis of BaO and Ru in oxidizing environment. The interaction of as-prepared $BaRuO_3$ with hydrogen at room temperature was examined by thermal desorption and X-ray diffraction experiments, showing that $BaRuO_3$ has the ability to uptake hydrogen in the bulk. The hydrogen interaction is discussed with respect to octahedral ruthenium local environment present in the oxide structure.

Addition of 1 mol% $BaRuO_3$ to MgH_2 was performed by ball milling. Hydrogen desorption properties were investigated by Sievert and DSC, connected with a H_2 detector. The H_2

desorbed from of the nano-structured materials is lower than the theoretical content in MgH_2, due to the presence of a non-reactive MgO layer. A remarkable increase of the H_2 desorption kinetics in nano-structured MgH_2 was observed with respect to bare MgH_2. The activation energy for hydrogen desorption from $MgH_2/BaRuO_3$ mixture was estimated by Arrhenius and Kissinger methods and a value around 130 $kJmol^{-1}$ and 90 $kJmol^{-1}$ was obtained, respectively.

Introduction

MgH_2 is an excellent material due to its high hydrogen storage capacity. However, the equilibrium dehydrogenation temperature is high, around 570 K under 1 bar of H_2 and the ab/desorption kinetics is undesirably slow [1-8]. A number of techniques has been applied to improve the ab/desorption kinetics of MgH_2, for example, ball-milling [9-11] with different additives e.g., transition metals (TM) [12-14] and transition metal oxides (TMO) [15-20]. The addition of niobia (Nb_2O_5), in particular, has demonstrated an increase of reactivity in MgH_2 with respect to H_2 uptake/release [9,21-25]. Recently, the interaction of hydrogen with MgH_2 in presence of ternary Mg-Nb oxides has been studied [26], suggesting a prominent effect for the system $Mg_3Nb_6O_{11}$. However, the exact role of additives on reaction mechanism still remained unclear. An empirical rule suggests that TM atoms (Nb, Cr, W etc.) having multiple valence states in corresponding TMOs, show better reaction efficiency [7,21]. In addition, the interaction of H_2 with TMOs has drawn attention in order to understand their specific role on H_2 ab/desorption reactions in MgH_2 [27-32]. In particular, it has been suggested that the occurrence of a hydrogen absorption in the additive oxide phase may facilitate the overcome of the MgO layer formed at the surface of the MgH_2 particles, leading to an improved reaction kinetics [25,26].

Chabanier et al. [33] performed electrochemical studies on RuO_2 and IrO_2 and suggested that these oxides show good electrocatalytic activity towards hydrogen evolution, leading to a

$RuO_2H_{0.09}$ and $IrO_2H_{0.03}$ phases. Shelef et al. [34] reported that $BaRuO_3$, after interaction with hydrogen (H_2 pressure 40 kPa) at room temperature (RT) for 6 days, absorbs 0.1 wt% hydrogen, corresponding to a $H_{0.3}BaRuO_3$ phase. These results suggest a specific investigation on the role of $BaRuO_3$ addition on hydrogen desorption from MgH_2.

In this paper, $BaRuO_3$ has been prepared by solid-state reaction following the synthetic approach reported in the literature [35]. A preliminary study on the hydrogen interaction with the oxide phases has been performed, showing a significant hydrogen absorption at room temperature. In addition, H_2 desorption kinetics in MgH_2 promoted by ball-milling with 1 mol% $BaRuO_3$ has been investigated. The activation energy for hydrogen desorption has been estimated from isothermal and scanning measurements. It turns out significantly lower than that obtained for the bare MgH_2 and comparable to those reported in the literature for different TMO additives [14,23].

Experimental

The starting materials used for solid-state synthesis of $BaRuO_3$ were commercially barium oxide (BaO) and ruthenium (Ru) (Sigma-Aldrich, 99% pure). The compound was prepared by heating a stoichiometric mixture of reagents with a rate of 5 K/min up to 1473 K and annealing for 24 hours in oxidizing environment. Reactive milling of pure $BaRuO_3$ was performed in a commercial Spex model-8000 Mixer/Mill with a ball-to-powder mass ratio of 15:1 under a hydrogen pressure of 0.5 MPa for 20 h. Hydrogen absorption in as-prepared $BaRuO_3$ was carried out at RT for 58 h with a hydrogen pressure of 6.5 MPa inside of a Sievert-type apparatus. 1 mol% of pure $BaRuO_3$ was added to 5 g of commercial MgH_2 (Alfa Aesar, Johnson Matthey Company, 98% purity, balance Mg) for ball-milling, carried out in a commercial Spex model-8000 Mixer/Mill for 12 h under a high purity Ar atmosphere. The milling run was carried out at 875 rpm by employing a special hardened steel vial and two

hardened steel milling balls with a ball-to-powder mass ratio of 7:1. Pure MgH_2 was ball milled under the same conditions for comparison.

Structural features of solid-state materials have been analyzed by X-ray diffraction (XRD) at RT with an X'PERT PRO diffractometer (Panalytical) with Cu Kα radiation. XRD patterns were collected in a step of 0.017 degree after accumulation of intensity data points in the range 10-100° for 1 h. Diffraction patterns were refined with Rietveld method using MAUD (Material Analysis Using Diffraction) program [36].

Hydrogen desorption properties were investigated by Thermal Programmed Desorption (TPD) coupled with a home-made heating apparatus to a quadruple Mass Spectrometer (MS, Pfeiffer Vacuum Prisma). Thermal desorption data were recorded during TPD measurements between 313 K and 1073 K with a heating rate of 7.5 K/min in high vacuum (10^{-6} bar) condition.

The samples were characterized by an AMC (Advanced Materials Corporation) instrument for hydrogen desorption at different programmed temperatures (573-653 K) in isothermal condition until reaching an equilibrium condition under a hydrogen pressure of 0.1 MPa. About 0.6 g sample were used for each measurement. Hydrogen desorption properties were also measured with a differential scanning calorimeter Perkin-Elmer DSC7. Measurements have been carried out with heating rate of 5, 10, 20 and 40 K/min. Two successive runs were performed and the data were subtracted from the signals of the second run defined as baseline.

Results and discussion

Pure $BaRuO_3$

The XRD pattern of the product after the solid state synthesis of BaO + Ru is shown in Figure 1 (pattern a). The use of a logarithmic scale is adopted for the analysis because intense and weak peaks may be equally important in order to correctly reconstruct the structure properties

of materials. Indeed, the shift of the ordinate variable among the patterns is operated simply by multiplication of intensity data points by a constant factor. With this simple manipulation the signal-to-background trend is maintained, when adopting the same collection strategy in the instrument as well as the similar protocol of sample preparation in terms of density and chemistry. The Rietveld fit to the pattern (R_{wp} = 2.1%) confirms the rhombohedral structure of $BaRuO_3$ (space group R-3m) with lattice parameters a = 5.752 (±0.001) Å and c = 21.623 (±0.003) Å, that closely correspond to reference values given by the Inorganic Crystal Structure Database (ICSD) file 10253, within experimental uncertainty. Crystal size and microstrain of the ternary oxide are >200 nm and < $3.9 \cdot 10^{-4}$, respectively, i. e., beyond the instrument resolution. The as-prepared $BaRuO_3$ compound was investigated by hydrogen and water desorption (TPD-MS) and results are reported in Figure 2. The curve of as-prepared sample is a flat baseline, indicating that no desorption phenomena related to water and hydrogen release occurred.

The XRD pattern registered after reactive milling of $BaRuO_3$ under H_2 atmosphere is shown in Figure 1 (pattern b). The ternary oxide transformed during reactive milling due to the interaction of hydrogen, so that mono/tri-hydrated barium hydroxides (25 wt% ± 3%) and metallic Ru (28 wt% ± 3%) were obtained, together with the parent oxide (47 wt% ± 5%). In addition, significant broadening of the diffraction peaks is observed due to formation of nanocrystalline solids (10-90 nm) during mechano-chemical treatment. The results suggests that reactive milling under H_2 promotes chemical reactions with $BaRuO_3$, leading to a reduction of Ru^{4+} to Ru^0 and to the formation of OH^- groups. The XRD pattern (not shown) remains rather similar after an annealing of the sample up to 950 K, suggesting that the observed reactions are irreversible. So, a milder hydrogenation process has been explored.

Figure 1 (pattern c) shows the XRD pattern of $BaRuO_3$ after interaction at RT with a H_2 pressure of 6.5 MPa for 58 h. With respect to the as-prepared pattern, the lower signal-to-

background ratio is due to peak distortion and broadening, on account for lattice parameter change of the rhombohedral structure. The XRD pattern was fit according to the Rietveld method (R_{wp} = 4.5%) and allowed the evidence of a consistent fraction (33 wt% ± 3%) of a new rhombohedral phase, with the same structure of $BaRuO_3$, but with lattice parameters elongated in the c direction (a = 5.755 (± 0.001) Å and c = 21.819 (± 0.003) Å,), together with a weak presence (7 wt% ± 1%) of a tetragonal phase, isostructural with $BaSrTiO_3$ compound (ICSD, file 54150). These effects are related to the interaction of the original phase with hydrogen. In addition, the average crystallite size (45 nm ± 4) of the distorted phase obtained after hydrogenation at 6.4 MPa is significantly reduced with respect to that of the as-prepared sample, together with an increase in the microstrain ($4.3 \cdot 10^{-3} \pm 2 \cdot 10^{-4}$). Being the rest of the mixture constituted by the parent $BaRuO_3$ rhombohedral phase, an incomplete hydrogenation reaction can be envisaged, in agreement with previous findings [34].

The TPD-MS spectra for hydrogen and water desorption from $BaRuO_3$ after hydrogen absorption at 6.4 MPa are shown in Figure 2. Desorption peaks related to hydrogen and water are observed in similar positions, at temperatures starting from 400 K and 750 K. Moreover, the hydrogen desorption peak intensity is about 30 times that related to water desorption, suggesting the occurrence of simple H_2 insertion in the crystal structure, rather than a chemical interaction with oxide anions.

The XRD pattern after TPD-MS of $BaRuO_3$ hydrogenated at RT under 6.4 MPa is shown in Figure 1 (pattern d). The single rhombohedral $BaRuO_3$ phase is assessed by the Rietveld refinement (R_{wp} =3.36%), with lattice parameters a = 5.750 Å and c = 21.611 Å, rather similar to those obtained for the as-prepared sample. The crystal size, above the resolution limit of 200 nm, is remarkably increased after TPD-MS measurement, due to the microstructure coarsening. These results suggest a full recovering of the original structural properties after TPD-MS measurement, indicating a reversibility of the hydrogenation process in $BaRuO_3$.

Shelef et al. [34] reported that $BaRuO_3$ absorbed 0.1 wt% hydrogen ($H_{0.3}BaRuO_3$) at RT after interaction with hydrogen (H_2 pressure 40 kPa) for 6 days. From the reported results, it is worth noting that $BaRuO_3$ is active to hydrogen absorption at RT even using much higher pressure (H_2 pressure 6.4 MPa). This behaviour has been already observed for other oxides, like $Mg_3Nb_6O_{11}$ [37], Nb_2O_5 and WO_3 [32].

The crystal structure of $BaRuO_3$ has been derived by the bond valence method [38]. The crystal is based on a layered rhombohedral structure, which is considered to be the stable form of $BaRuO_3$ at ambient pressure, confirmed by Rietveld refinement of as-prepared sample (Figure 1). The unary cell of $BaRuO_3$ is formed by units of three face-sharing RuO_6 octahedra, which are connected to one another by corner sharing. The crystalline Ru (IV) oxide (RuO_2) has the rutile-type structure and it is also composed of RuO_6 octahedra. Recently, attention has been directed toward the use of RuO_2 electrode as an activated cathode for H_2 evolution. This oxide shows good electrocatalytic activity for H_2 evolution and excellent resistance to deactivation due to deposition of metallic impurities [33]. The fact behind H_2 interaction with RuO_2 is that H_2 can penetrate into the RuO_2 structure in the absence of polarization. Moreover, the measured H/Ru ratio suggests that surface hydroxylation occurs with no bulk modification. On the contrary, for $BaRuO_3$, H_2 absorption may occur also into the bulk of the material. In fact, the expansion of the unit cell has been noticed along the c-axis after H_2 interaction (Figure 1), strongly suggesting that H_2 is inserted in the a-b plane of the unary cell. The oxygen atoms of the shared faces in each unit are pulled together, thus providing a 'shielding effect' that reduces the Ru-Ru interactions, facilitating H_2 incorporation and diffusion inside the structure.

Hydrogen absorption and desorption in $BaRuO_3$ may be discussed according to reactions proposed for H_2 interaction with Nb_2O_5 [39,40]:

$$BaRuO_3 + xH^+ + xe^- \rightarrow H_xBaRuO_3 \qquad (1)$$

$$H_xBaRuO_3 \rightarrow BaRu^{4+}O_3 + x/2H_2 \quad (2)$$

$$H_xBaRuO_3 \rightarrow BaRu_x^{3+}Ru^{4+}_{1-x}O_{3-x/2} + x/2H_2O \quad (3)$$

In reaction 1, ionization of the incoming hydrogen occurs with release of electrons which can delocalize either into the conduction band of the solid or on a ruthenium ion, which changes its oxidation state. The residual H^+ is stabilized by oxygen ions of the lattice producing OH^- groups. Upon annealing, two possible reactive channels can be followed. In the first case (reaction 2), the process leads to hydrogen desorption and tends to restore the initial oxidation state of the transition metal. In the second case (reaction 3), the process leads to water desorption and the metal ion is partially reduced. So, $BaRuO_3$ after contact with molecular hydrogen may be partially reduced by formation of hydroxyl groups and perhaps of hydride ions. Consequently, both hydrogen and water desorption can be explained on the basis of different bonding energy of OH^- groups at various crystallographic sites.

In conclusion, $BaRuO_3$ is not at all inert while interacting with hydrogen. This peculiar behavior, reminiscent of some properties of the bronze family and Nb_2O_5 [32], suggests a possible active chemical role played by $BaRuO_3$ in the mixed $MgH_2/BaRuO_3$ system.

MgH_2+$BaRuO_3$ mixture

The XRD pattern of physically mixed MgH_2 with $BaRuO_3$ additive is shown in Figure 3 (bottom curve). In the parent MgH_2 a small contamination (lower than 2 wt.%) of hexagonal Mg was found. The XRD pattern in Figure 3 (upper curve) refers to the mixture after ball milling for 12 h. The intensity of MgH_2 diffraction profiles is affected by a large amount of peak broadening. The phase analysis evidences that tetragonal MgH_2 is the main phase present (57 wt.%) but 23 wt.% of the sample is under the form of a γ-MgH_2 orthorhombic phase, together with a non-negligible quantity of periclase MgO (15 wt.%). The remaining 5 wt.% of the mixture is attributed to $BaRuO_3$, showing diffraction peaks with a lower degree of broadening, as expected from the brittleness of the oxide phase. The nominal amount of

$BaRuO_3$ present in MgH_2 is 9.9 wt% (1 mol%). The reduced amount of pure $BaRuO_3$ after ball milling might be related to an interaction of the additive with the MgO layer surrounding the MgH_2 particles, suggesting a possible active role of the additive in the hydrogen sorption processes.

The results of the PCI experiment of H_2 desorption from commercial MgH_2, ball milled MgH_2 and $MgH_2/BaRuO_3$ ball milled mixture at 593 K under 0.1 MPa of hydrogen pressure are reported in Figure 4a. Because the total amount of hydrogen released from various samples is different, the results are reported as a transformed fraction as a function of time for better comparison. Commercial MgH_2 shows very slow desorption rate, whereas ball milled MgH_2 desorbs hydrogen much faster, as already reported in the literature [10]. $MgH_2/BaRuO_3$ ball milled mixture shows better desorption properties, due to the effect of ball milling and to the presence of the additive. Desorption curves for $MgH_2/BaRuO_3$ ball milled mixture from 653 to 573 K under 0.1 MPa H_2 pressure are reported in Figure 4b, where the hydrogen release at various temperatures is reported as a function of time. The nominal hydrogen content in $MgH_2/BaRuO_3$ ball milled mixture is 6.9 wt.%, respectively. The total amount of hydrogen desorbed from the samples is lower than the maximum nominal capacity, likely due to the presence of a non-reactive MgO layer on the surface of the powders.

The activation energy (*Ea*) of H_2 desorption may be estimated from the Arrhenius equation:

$$k = A \cdot exp(-Ea/RT) \qquad (4)$$

where *k* is a temperature dependent reaction rate constant, *A* is the pre-exponential factor, *R* is the gas constant and *T* is the absolute temperature. The *k* values can be obtained by analyzing the isothermal H_2 desorption curves with appropriate kinetic rate expressions, which are derived from the corresponding solid-state reaction mechanism models such as nucleation, geometrical contraction, diffusion and various reaction order models. Therefore, the model parameters obtained from the fitting of desorption data with suitable models also reflects the

desorption mechanism. So, the desorption curves have been analyzed using the Johnson-Mehl-Avrami (JMA) equation [41-43]:

$$\alpha(t) = 1 - exp[-(kt)^n] \quad (5)$$

where α is the phase fraction transformed at time t and n is the Avrami exponent. The JMA fitting of experimental data of hydrogen desorption from $MgH_2/BaRuO_3$ ball milled mixture are shown in Figure 4b as continuous lines. The obtained values of n and k are reported in Figure 5 as a function of the inverse temperature, together with the same results obtained for commercial MgH_2 and ball milled MgH_2. From the linear fit of $ln(k)$ as a function of $1/T$, the Ea values were obtained according to eq. (4) and turned out equal to 170 $kJmol^{-1}$, 140 and 130 $kJmol^{-1}$ for commercial MgH_2, ball milled MgH_2 and $MgH_2/BaRuO_3$ ball milled mixture, respectively. Due to the progressive approaching of the equilibrium temperature at the desorption pressure (0.1 MPa) on decreasing temperatures [26], a correction of the kinetic constants obtained at various temperatures with a constant pressure has been suggested [44]. In the case of a constant sample geometry, the kinetic constant, k(T,P), obtained from the JMA analysis (eq. 5) can be normalized by the driving force, $g(P/P_{eq})$, so that a purely kinetic constant, h(T), can be obtained. The driving force depends on the ratio P/P_{eq}, where P is the pressure of the desorption experiment (0.1 MPa in these experiments) and P_{eq} is the equilibrium pressure at the temperature of the experiment [44, 45]. Attempts to apply the correction for the driving force led to a significant decrease of the correlation coefficient for the linear regression in the Arrhenius plot of Figure 5, with the consequence of unreasonable values for the activation energy. So, row values of the kinetic constant have been taken for the calculation of the activation energies, in agreement with similar studies [10,46]. The application of the JMA equation to the hydrogen desorption in MgH_2 lead to different values for the Avrami coefficient [43,46], that have been associated to various reaction mechanisms. From the results shown in Figure 5, it appears clear that the n values increase for decreasing

temperature. The temperature dependence of the n value might be related to the change in the driving force for the phase transformation, as discussed above. In all cases, n values turn out in the range between 1 and 3. In addition, n values are the highest for commercial MgH_2, become lower for the ball milled MgH_2 and are the lowest for $MgH_2/BaRuO_3$ ball milled mixtures, suggesting an active role of the ball milling process and of the additive in changing the reaction mechanism for hydrogen desorption.

The results of hydrogen desorption measured by DSC for $MgH_2/BaRuO_3$ ball milled mixture at different heating rates (5, 10, 20 and 40 K/min) are shown in Figure 6. An apparent endothermic signal is observed in correspondence of the hydrogen desorption, because of the change in thermal conductivity of the gas surrounding the sample [47]. For pure MgH_2, a single DSC signal is usually obtained for hydrogen desorption [43]. On the contrary, for the ball milled $MgH_2/BaRuO_3$ mixture, multiple peaks signal appeared (Figure 6), suggesting the occurrence of hydrogen desorption from different crystallographic sites or phases.

The activation energy for hydrogen desorption has been estimated by Kissinger method according to [48]:

$$d(ln(\beta/T_p^2)/d(T_p^{-1})=-Ea/R \qquad (6)$$

where β is the heating rate and T_p is the peak temperature in the DSC trace. The obtained Ea values were 140 $kJmol^{-1}$, 120 $kJmol^{-1}$ and 90 $kJmol^{-1}$ for commercial MgH_2, ball milled MgH_2 and $MgH_2/BaRuO_3$ ball milled mixture, respectively.

The Ea values for hydrogen desorption from powdered MgH_2 with coarse microstructure reported in the literature range from 300 $kJmol^{-1}$ [44] down to 140 $kJmol^{-1}$ [11]. The ball milling itself accelerates the reaction of hydrogen desorption from MgH_2 simply because of a reduced diffusion path, but it generally introduces a significant amount of MgO, forming a diffusion barrier at the surface of the particles. In this case, a value of activation energy around 120 $kJmol^{-1}$ range has been obtained, in good agreement with results previously

reported in the literature [42]. The presence of the additive promotes the hydrogen insertion inside the oxide layer, further reducing the *Ea* values. In fact, values around 60-70 kJmol^{-1} have been reported when Nb_2O_5 is added during ball milling [22,23]. In particular, during the hydrogen sorption cycling of the MgH_2/ Nb_2O_5 mixture, a ternary $Mg_3Nb_6O_{11}$ compound is formed at the surface [25], which has been shown to be able to absorb H_2 reversibly in the bulk [37].

After $BaRuO_3$ addition, the *Ea* value for hydrogen desorption from MgH_2 becomes significantly lower with respect to that obtained for the commercial powder. In both cases, the *Ea* values obtained from isothermal desorption measurements turn out higher than those obtained from scanning measurements, likely because of the different experimental conditions (i.e. H_2 pressure, driving force), which might affect the reaction mechanism. On the other hand, the peculiar properties of $BaRuO_3$ as "oxide bronze" seems to be related to its role in promoting hydrogen desorption. In fact, the mixing of $BaRuO_3$ with MgO at the surface of the particles during ball milling, might produce preferential paths for hydrogen, which turn out in a decreasing of the apparent activation energy. So, it can be concluded that the $BaRuO_3$ addition during ball-milling of MgH_2 promotes the formation of an active system with respect to H_2 release, as already demonstrated for other oxide systems.

Conclusions

In this paper it has been demonstrated that the $BaRuO_3$ absorbs hydrogen at RT and 6.4 MPa H_2 pressure, leading to rhombohedral distorted phase, with a c-axis elongated with respect to the parent structure. During TPD, the hydrogenated oxide phase releases mainly hydrogen, coupled with a small amount of water, suggesting the occurrence of an oxide-bronze behaviour. The rate of the H_2 desorption in MgH_2 is accelerated by ball milling with addition of $BaRuO_3$. In particular, the ball milled MgH_2/$BaRuO_3$ mixture showed a value of the

apparent activation energy for hydrogen desorption significantly lower with respect to that obtained for commercial MgH_2, likely due to a change in the reaction mechanism. The peculiar properties of $BaRuO_3$ as a promoter for hydrogen desorption from MgH_2 have been correlated with its aptitude to absorb hydrogen in the bulk structure.

References

[1] B. Sakintuna, B. Weinberger, F. Lamari-Darkrim, M. Hirscher, B. Dogan, Int. J. Hydrogen Energy 32 (2007) 1121.

[2] L. Zaluski, A. Zaluska, J. O. Ström-Olsen, J. Alloys Compd. 253 (1997) 70.

[3] H. Imamura, K. Masanari, M. Kusuhara, H. Katsumoto, T. Sumi, Y. Sakata, J. Alloys Compd. 386 (2005) 211.

[4] M. Zhu, H. Wang, L. Z. Ouyang, M. Q. Zeng, Int. J. Hydrogen Energy 31 (2006) 251.

[5] A. Zaluska, L. Zaluski, J. O. Ström-Olsen, Appl Phys A. 72 (2001) 157.

[6] R. Wiswall, in: G. Alefeld and J. Völkl, Editors, Topics in Applied Physics, Vol.29, Hydrogen in Metals 2, Springer, Berlin/Heidelberg (1978), p. 209.

[7] Y. Fukai, The metal–hydrogen, system. Basic bulk properties, Springer Series in Material Science Vol. 21, Springer-Verlag, Berlin (1993).

[8] L. Schlapbach, A.Zuttel, Nature, 414 (2001) 353.

[9] K. F. Aguey-Zinsou, J. R. A. Fernandez, T. Klassen, R. Bormann, Int. J. Hydrogen Energy 32 (2007) 2400.

[10] J. Huot, M. L. Tremblay, R. Schulz, J Alloys Compd. 356 (2003) 603.

[11] D. Fatay, A. Revesz, T. Spassov, J. Alloys Compd. 399 (2005) 237.

[12] J. L. Bobet, E. Akiba, Y. Nakamura, B. Darriet, Int. J. Hydrogen Energy 25 (2000) 987.

[13] C. X. Shang, M. Bououdina, Z. X. Guo, J. Alloys Compd. 349 (2003) 217.

[14] J. Huot, J. F. Pelletier, L. B. Lurio, M. Sutton, R. Schulz, J. Alloys Compd. 348 (2003) 319.

[15] M. Q. Fan, L. X. Sun, Y. Zhang, F. Xu, J. Zhang, H. L. Chu. Int. J. Hydrogen Energy 33 (2008) 74.

[16] A. Patah, A. Takasaki, J. S. Szmyd, Int. J. Hydrogen Energy 34 (2009) 3032.

[17] F. Dolci, M. Baricco, P. P. Edwards, E. Giamello, Int. J. Hydrogen Energ. 33 (2008) 3085.

[18] C. Zhi, T. Chao, P. Hui, Y. Huabin, Int. J. Hydrogen Energy 35 (2010) 8289.

[19] W. Oelerich, T. Klassen, R. Bormann, J. Alloys Compd. 315 (2001) 237.

[20] K. S. Jung, E. Y. Lee, K. S. Lee, J. Alloys Compd. 421 (2006) 179.

[21] G. Barkhordarian, T. Klassen, R. Bormann, Scripta Mater. 49 (2003) 213.

[22] G. Barkhordarian, T. Klassen, R. Bormann, J. Alloys Compd. 364 (2004) 242.

[23] N. Hanada, T. Ichikawa, S. Hino, H. Fujii, J. Alloys Compd. 420 (2006) 46.

[24] G. Barkhordarian, T. Klassen, R. Bormann, J. Phys. Chem. B 110 (2006) 11020.

[25] O. Friedrichs, J. C. Sanchez-Lopez, C. Lopez-Cartes, T. Klassen, R. Bormann, A. Fernandez, J. Phys. Chem. 110 (2006) 7845.

[26] M. W. Rahman, A. Castellero, S. Enzo, S. Livraghi, E. Giamello, M. Baricco J. Alloys Compd. 509S (2011) S438.

[27] K. Schlberg, S. T. Pantelides, S. J. Pennycook, J. Am. Chem. Soc. 123 (2001) 6609.

[28] S. Nieto, R. Polanco, R. Roque-Malherbe, J. Phys. Chem. C 111 (2007) 2809.

[29] Q. Wan, C. L. Lin, X. B. Yu, T. H. Wang, Appl. Phys. Lett. 84 (2004) 124.

[30] S. H. Lim, J. Luo, Z. Zhong, W. Ji, J. Lin, Inorg. Chem. 44 (2005) 4124.

[31] F. Dolci, M. Di Chio, M. Baricco, E. Giamello, J. Mater. Sci. 42 (2007) 7180.

[32] F. Dolci, M. Di Chio, M. Baricco, E. Giamello, Mater. Res. Bull. 44 (2009) 194.

[33] C. Chabanier, D. Guay J. Electroanal. Chem. 570 (2004) 13.

[34] M. Shelef, R. A. D.Betta, K. Otto, J. Inorg. Nucl. Chem. 38 (1976) 99.

[35] P. C. Donohue, L. Katz, R. Ward, Inorg Chem. 4 (1965) 306.

[36] L. Lutterotti, S. Matthies, H–R. Wenk, A. J. Schulz, J. Richardon, J. Appl. Phys. 81 (1997) 594. MAUD is available at http://www.ing.unitn.it/~maud.

[37] M. W. Rahman, S. Livraghi, F. Dolci, M. Baricco, E. Giamello, Int. J. Hydrogen Energy 36 (2011) 7932.

[38] A. Santoro, I. N. Sora, Q. Huang, J. Solid State Chem. 151 (2000) 245.

[39] B. Reichman, A. J. Bard. J. Electrochem Soc. 127 (1980) 241.

[40] M. A. B. Gomes, L. O. D. Bulhoes, S. C. De Castro, A. J. Damiao, J. Electrochem. Soc. 137 (1990) 3067.

[41] M. Avrami, J. Chem. Phys. 7 (1939) 1103.

[42] J. Huot, G. Liang, S. Boily, A. Van Neste, R. Schulz, J. Alloys Compd. 293–295 (1999) 495.

[43] J. F. Fernandez, C. R. Sanchez, J. Alloys Compd. 356-357 (2003) 348.

[44] J. F. Fernandez, C. R. Sanchez, J. Alloys Compd. 340 (2002) 189.

[45] L. Pasquini, E. Callini, E. Piscopiello, A. Montone, M. Vittori Antisari, E. Bonetti, Appl. Phys. Lett. 94 (2009) 041918.

[46] T. R. Jensen, A. Andreasen, T. Vegge, J. W. Andreasen, K. Stahl, A. S. Pedersen, M. M. Nielsen, A. M. Molenbroek, F. Besenbacher, Int. J. Hydrogen Energy 31 (2006) 2052.

[47] M. Di Chio, S. Livraghi, M. Baricco J. Alloys Compd. 426 (2006) 180.

[48] H. E. Kissinger, Anal. Chem. 29 (1957) 1702.

Figure captions

Figure 1. The XRD pattern of: $BaRuO_3$ powders as prepared from solid state synthesis of BaO+Ru (pattern a); $BaRuO_3$ powders after reactive milling under 0.5 MPa of hydrogen (pattern b); $BaRuO_3$ powders subjected to a hydrogenation at 6.5 MPa (pattern c) and $BaRuO_3$ powders obtained after TPD of hydrogenated sample (pattern d). Experimental data points are dots, full lines are the result of the Rietveld fit to the data. The hkl sequence of peaks for rhombohedral $BaRuO_3$ has been reported at the bottom of the figure.

Figure 2. TPD-MS profiles as a function of temperature for $BaRuO_3$ powders as-prepared (dashed lines) and after hydrogen loading at 6.5 MPa (continuous lines). H_2 and H_2O desorption are reported in top and bottom figure, respectively. Note the different scale values of the graphs.

Figure 3. XRD patterns of the mixtures of 1 mol% of $BaRuO_3$ and commercial MgH_2 powders as mixed (bottom curve) and subjected to a ball milling treatment of 12 h (top pattern). Experimental data points are dots, full lines are the result of the Rietveld fit to the data. The as-mixed mixture displays weak presence of hexagonal magnesium phase. In the ball milled specimen it was assessed the weak presence of periclase MgO and of a γ-MgH2 orthorhombic phase.

Figure 4. Hydrogen desorption measured with a Sievert-type equipment as a function of time at hydrogen pressure of 0.1 MPa . Top, figure a: comparison among desorption at 593 K from as-received MgH_2 (squares), ball milled MgH_2 (circles) and $MgH_2/BaRuO_3$ ball milled mixture (triangles). Dashed lines are a guide for the eyes. Bottom, figure b: desorption from $MgH_2/BaRuO_3$ ball milled mixture at various temperatures, as indicated in the figure. Points: experimental data. Lines: fitting curves on the basis of eq. (5).

Figure 5. Rate constant, k (full points), and Avrami coefficient, n (open points), as a function of the inverse temperature for commercial MgH_2 (squares), ball milled MgH_2 (circles) and $MgH_2/BaRuO_3$ ball milled mixture (triangles).

Figure 6. DSC traces as a function of temperature for hydrogen desorption from $MgH_2/BaRuO_3$ ball milled mixture at various heating rates, as reported in the graphs.

Figure 7. Kissinger plot for commercial MgH_2 (squares), ball milled MgH_2 (circles) and $MgH_2/BaRuO_3$ ball milled mixture (triangles) based on the results of DSC measurements.

***Highlights**

- Interaction of $BaRuO_3$ with hydrogen studied.
- $BaRuO_3$ is able to release hydrogen after absorption.
- A distorted rhomohedral phase is formed in $BaRuO_3$ after hydrogen absorption.
- A mixture of $BaRuO_3$ with MgH_2 is able to desorb hydrogen much faster than the parent materials.
- The interaction of hydrogen with the oxide additive is a crucial aspect for improving the hydrogen desorption rate.

Figure(s)

Baricco et al. Figure 1

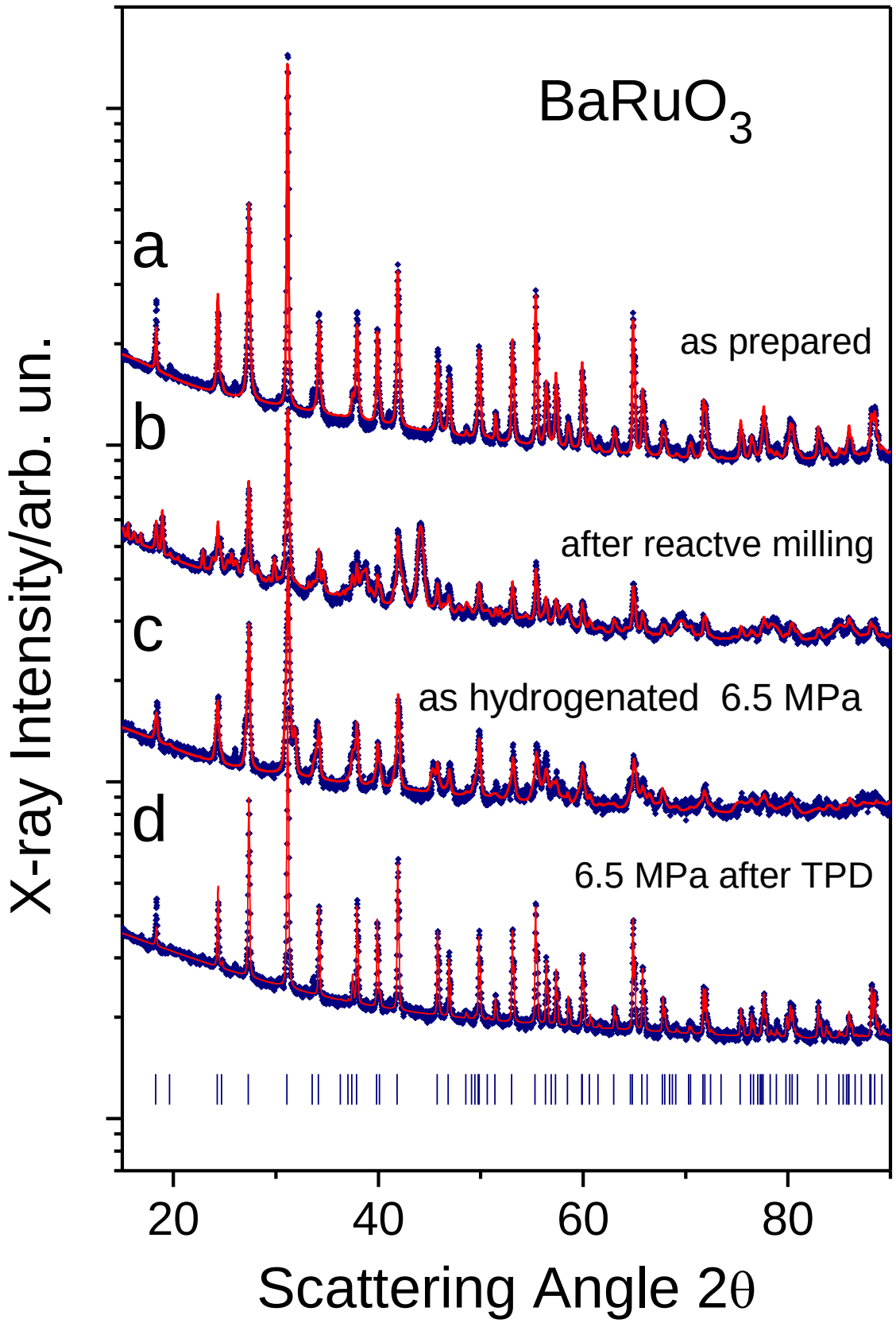

Baricco et al. Figure 2

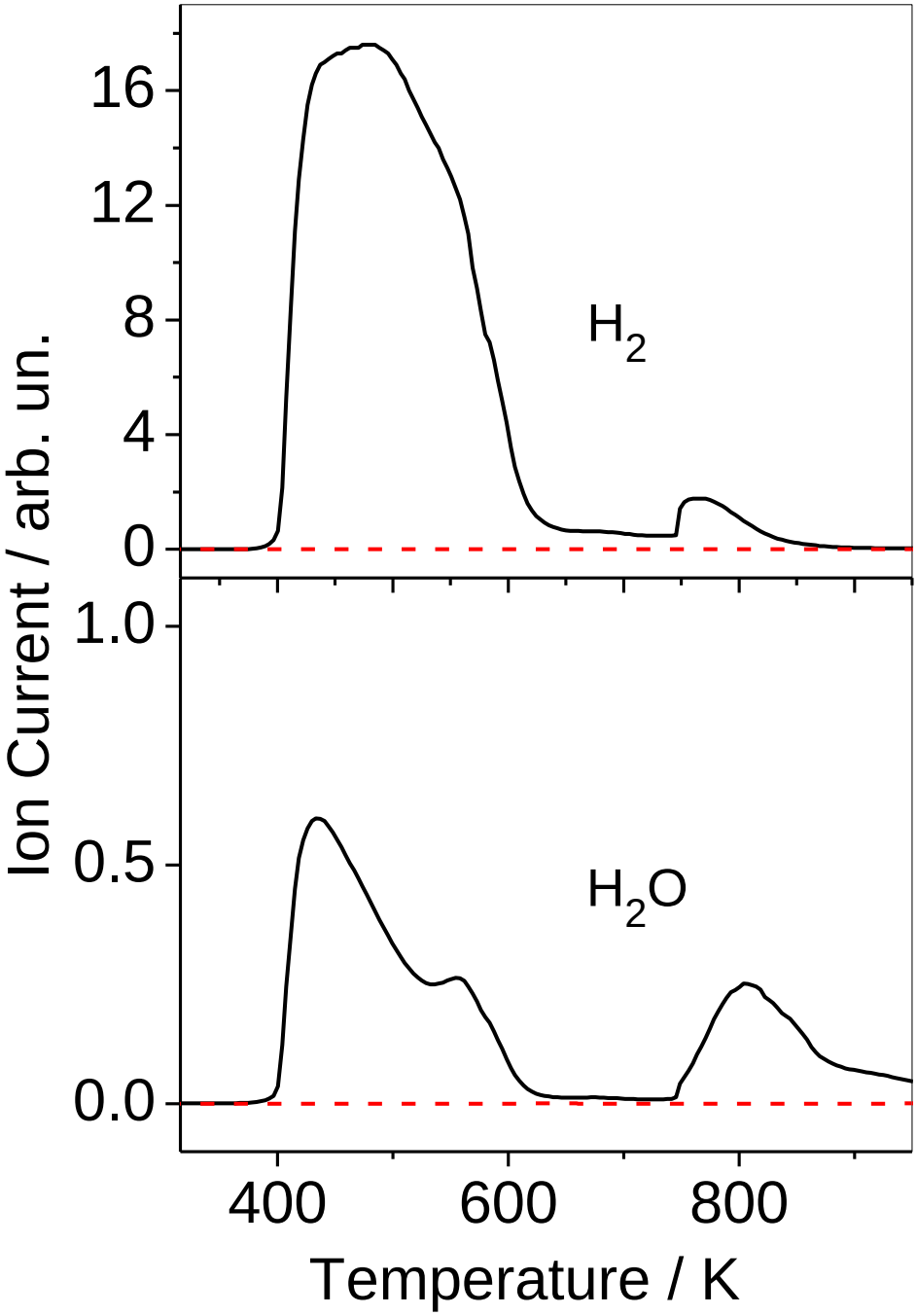

Baricco et al. Figure 3

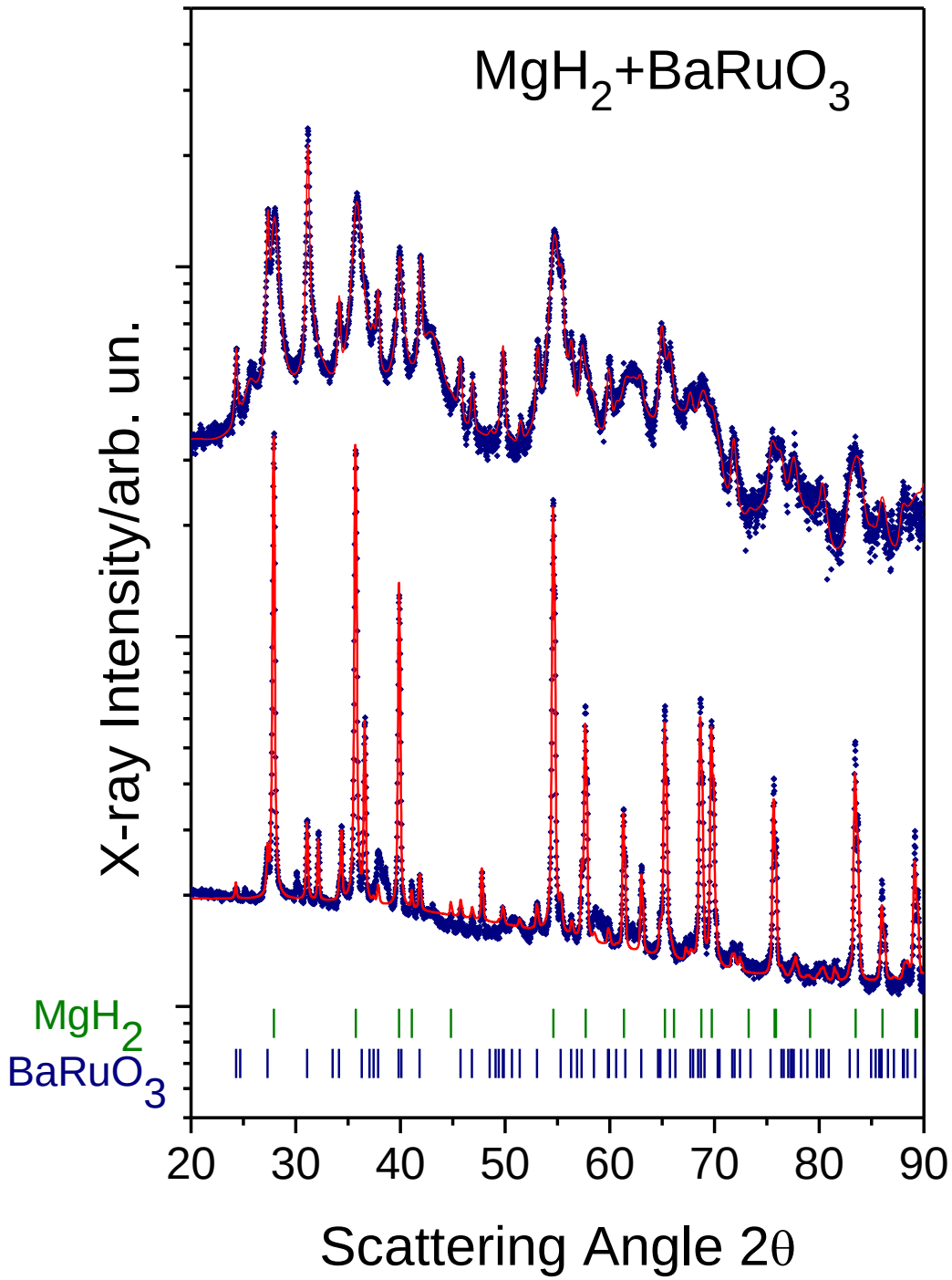

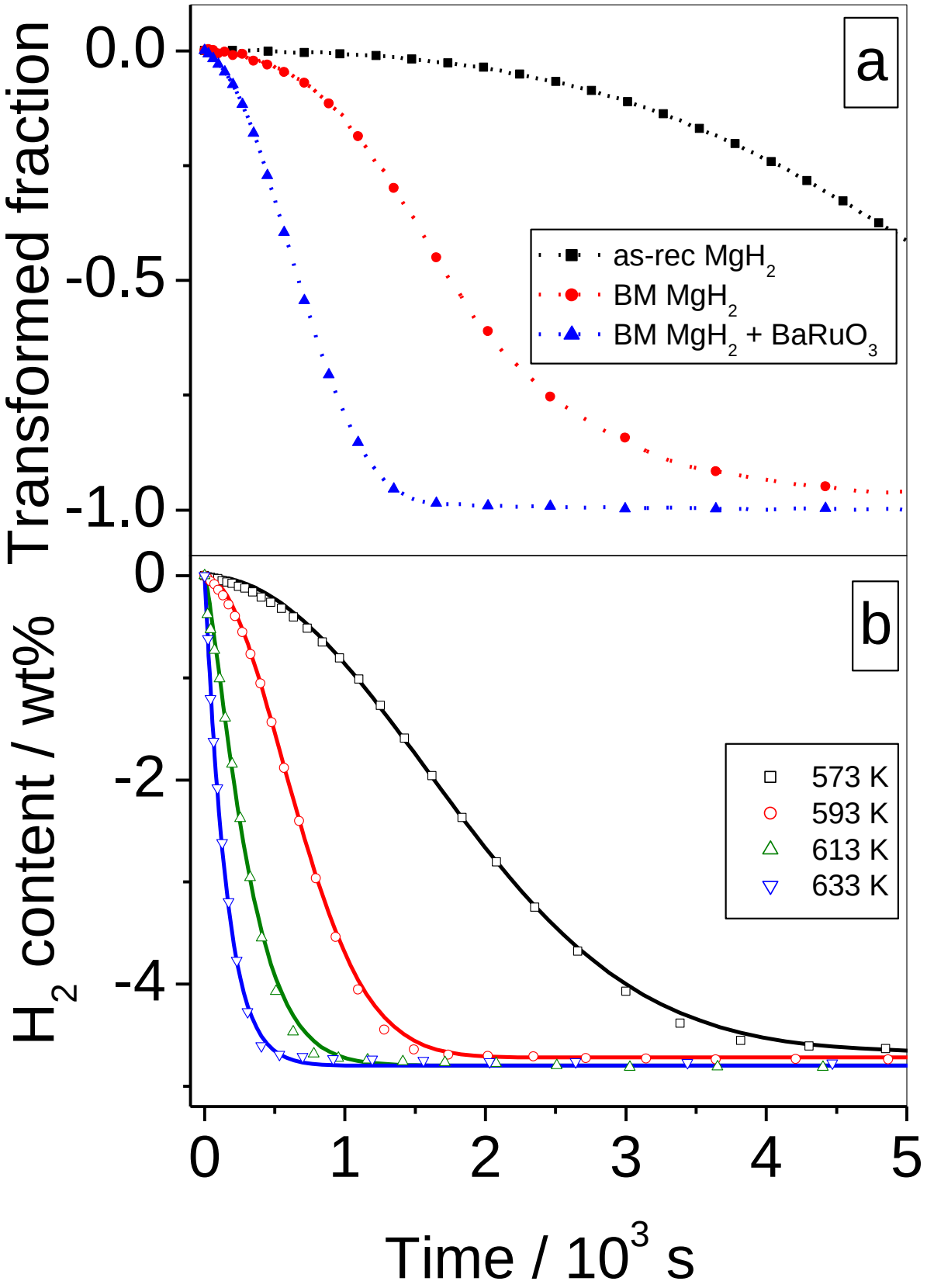
a
b
Transformed fraction
H2 content / wt%
0.0
-0.5
-1.0
0
-2
-4
as-rec MgH2
BM MgH2
BM MgH2 + BaRuO3
573 K
593 K
613 K
633 K
0
1
2
3
4
5
Time / 10^3 s

Baricco et al. Figure 5

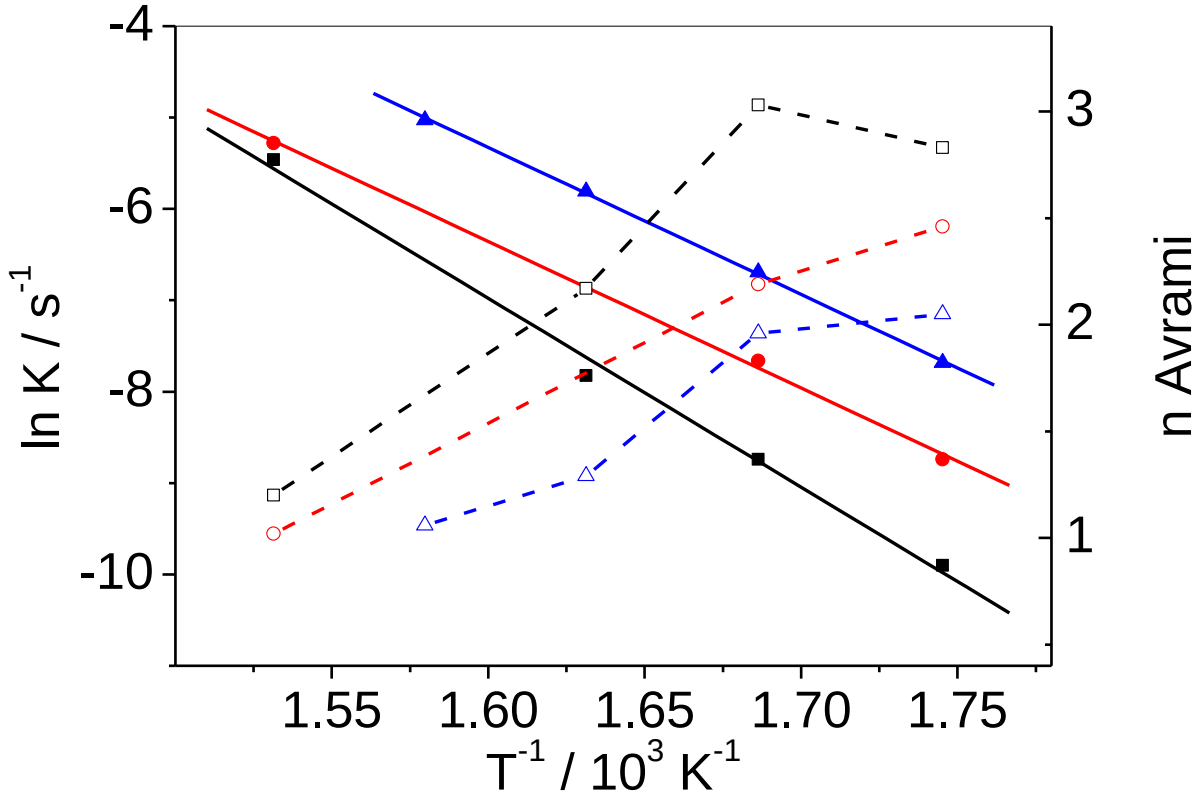

Baricco et al. Figure 6

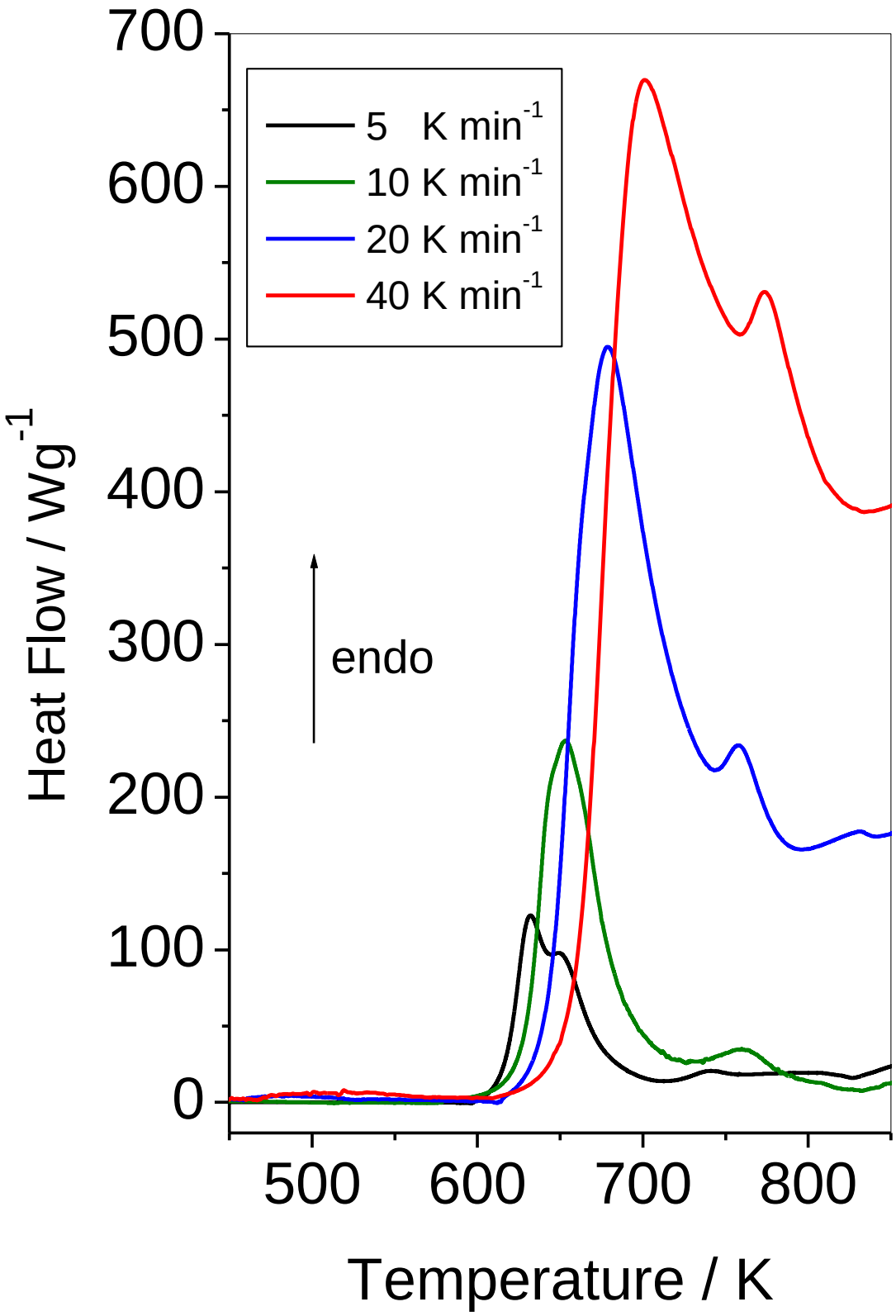

Baricco et al. Figure 7